Mechanically Tunable Ultrasonic Metamaterial Lens with Subwavelength Resolution at Long Working Distances for Bioimaging

Teng Yang,[1,2] Yuqi Jin,[1,3] Tae-Youl Choi,[3] Narendra Dahotre,[2,4] and Arup Neogi[1,4*]

[1]*Department of Physics, University of North Texas, PO Box 311427, Denton, TX 76203, USA*

[2]*Department of Materials Science and Engineering, University of North Texas, 3940 North Elm Suite F101, Denton, Texas 76207, USA*

[3]*Department of Mechanical and Energy Engineering, University of North Texas, 3940 North Elm Suite F101, Denton, Texas 76207, USA*

[4]*Center for Agile and Adaptive Additive Manufacturing, 3940 North Elm Suite F101, Denton, Texas 76207, USA*

[*]*Corresponding author: Arup Neogi. arup@unt.edu*

Abstract: In this study, a novel acoustic doublet meta-material lens has been designed and tested to demonstrate both a far-field focal point and ultra-long collimation characteristics past the Fresnel zone. The switching of the two behaviors can be adjusted by a simple linear mechanical translation of one of the lens units. The doublet lens can focus the sound wave beyond 38λ away from the experiment's lens, which is farther than any existing ultrasonic transducer or meta-lenses lenses. In terms of collimating behavior, the doublet lens is a unique metamaterial lens that experimentally demonstrates a long and narrow collimating beam over 70λ. Besides the design and characterization, the meta-lens have been used to detect real objects, including inorganic and organic matter. A subwavelength spatial resolution has been demonstrated. The detection limit was 0.26 λ in the monostatic setup and 0.62 λ in a bistatic experimental setup. This lens demonstrates super-resolution detection capabilities at distances of 42 λ and can enable ultrasonic diagnostics deep within a material or a biological tissue. The experimental performance of the doublet meta-material lens illustrated its potential to apply acoustic metamaterial elements in a practical imaging application, including the detection of biological tissues

Keywords: ultrasonic focusing, ultrasonic collimation, acoustic metamaterials, super-resolution detection.

1. Introduction

Phononic crystal (PC) is one of the approaches to modify the propagation of the sound wave. PC is periodic structures composed of two or more different materials, where the propagation can be controlled by the effective elastic properties of the phononic crystal. The artificial periodic scatter within the background material affects acoustic band structures like those in electronic and photonic crystals [1]. In the first transmission band, a phononic crystal acts as an effective medium with linear dispersion relation. The range of the waves' linear dispersion enables the phononic crystal to serve as an effective medium within the first transmission band.

Besides, the phase and group velocity of a traveling wave may not correlate beyond this homogenization limit in a PC. It leads to hyperbolic and elliptical metamaterials [2, 3]. The dispersion outside homogenization limits can also be strongly non-linear at certain incident angles of the wave. It can engineer artificial materials to exhibit anomalous gradient index effects [4], called gradient index lens.

Acoustic metamaterials lens (meta-lens) above the first transmission band have an effective index of refraction below 1.0 and can even approach an effective negative index of refraction [5]. The behavior is usually achieved in the periodic structure such as phononic crystals based meta-lens. The conventional negative index of refraction in acoustic metamaterial was achieved by negative effective-mass and bulk modulus [6]. In the two materials compositions, the negative index of refraction, negative wave group velocity can be achieved using two well-coupled resonant modes [7, 8]. In solid-liquid combination, the coupled-modes is easier to achieve. The effective refraction index in the solid-liquid phononic crystal based metamaterial cannot be deduced from a simple equation. The index is dependent on the frequency, filling fraction, lattice shape, and composition materials. In the second or higher transmission band, the effective index of refraction is also incident wave angle-dependent. The effective index of refraction of a similar structure phononic crystal has been numerically and experimentally analyzed by simulation of an existing study [9]. The meta-lens with incoherent waves offer sub-wavelength resolution, suitable solution to improve the resolution of ultrasound detection, and elastography [10, 11, 12] at low frequency to enhance the penetration depth with exceptional lateral resolution.

In this study, we present a PC based doublet acoustic meta-lens providing both super long collimation and tunable far focal points by simple linear mechanical translation. The simple mechanical translation tunability is more controllable than thermal [13] or electromagnetic [14] methods. The focusing/collimating tunable functionality has never been reported in the existing literature. We simulated and experimentally observed the doublet lens system's tunable focusing behavior in section 2.2 and 3.1. The focusing behavior of this doublet-lens has been compared with existing reports shows excellent focal length. The doublet lens can experimentally focus ultrasonic waves to a distance of 42.3λ to 36.5λ away from the lens's front edge by linear mechanical motion. Moreover, the doublet-lens can be applied to realize a 71λ long collimation beam to enhance ta single element plane wave transducer's energy density in the far-field and be used for practical ultrasound detection or imaging applications.

In practical ultrasound detection or imaging applications, multi-elements phased-array approaches high resolution based on advanced signal processing. The sensitive target size is still much larger than one wavelength. Alternatively, phononic metamaterials can be used to achieve super-resolution detection of characterizing objects smaller than the operating wavelength without advanced data acquisition or image processing. The initial studies on the 2-dimensional sonic crystals lens used hexagonal arrays of steel cylinders were based on a point source and are challenging to realize experimentally [15]. A negative index flat lens with the resolution at the focal point approaching $\lambda/50$ was realized using a 3D holey-structured metamaterial [16] in the near field in one of the reported studies. However, the super-resolution beam is generally confined to the evanescent wave field ($\leq 1\ \lambda$) of the system or within a few wavelengths ($\sim 5\ \lambda$), which makes the lenses impractical [17].

Our proposed PC-based doublet acoustic meta-lens performed real detection on both inorganic and organic materials at far-field in this study. In the distances about 15λ, the doublet-lens achieved the resolution up to 0.26 λ in object-size and 0.58 λ in object-spacing of inorganic material samples in a monostatic setup in section 3.3. In the super far-field detection, 70λ+ away from the second lens, the doublet-lens can still image an object with sub-wavelength resolution (0.88λ) of object size and 1.15λ resolution of object spacing in both inorganic and organic materials by bistatic setup.

2. Design of Metamaterial Lens and Numerical simulation

2.1. Design of Metamaterial Lens

The doublet-lens system is composed of two 2D phononic crystal metamaterial lenses. The phononic crystal structure's focusing behavior is based on its negative-index at a specific frequency that results in beam-splitting [18, 19]. A flat phononic crystal based meta-lens is the most conventional design that has been used for the focusing of acoustic waves. The focal length of a lens can be modified using a triangular or a convex-contour-like arrangement of the scatters [3]. In this work, the doublet-lens design was modified. The first element, which is a plano-convex lens, was used to diverge the incident wave. The second element – a flat meta-lens is used to focus the divergent beam as a conventional metamaterial lens. The advantage of focusing the divergent source beam from the first lens is that it enables a long distant focal point. As in a conventional optical lens, the second element's focusing point in the lens is analogous to the f-number of the optical system. The ratio of the focal length to the diameter of the entrance pupil width (or the clear aperture) can be controlled in this configuration by modifying the distance between the two lens elements. The width of the source beam is limited by the aperture of the piezoelectric transducer source. It also depended on the selected operating frequency and was verified by the phased maps discussed in section 3.1.

Standard 1/16 inch (1.6mm) stainless steel rods were chosen to construct a phononic crystal with a 50.1% filling fraction in water as an ambient medium. The square phononic crystal lattice is made of stainless-steel rod scatters with a lattice constant a=1.96mm and radius r=0.8mm. The first element of the lens is a trapezoid shape lens with the base of 7a on the incident side, the base of 29a on the other side, and a height of 10a. The second lens is a rectangle shape lens with a base of 39a and a height of 5a. The steel rods are 4 inches tall, which is 39λ in order to approach the behavior close enough to a 2D crystal in the calculated band structure. In the setup, the distance between the source transducer surface to the second lens is always fixed as 100mm. The first lens can move linearly between the transducer and the second lens to locate inside or outside the source transducer's near field zone. The concept of non-flat shape phononic meta-lens is described as a combination of lens geometry [20].

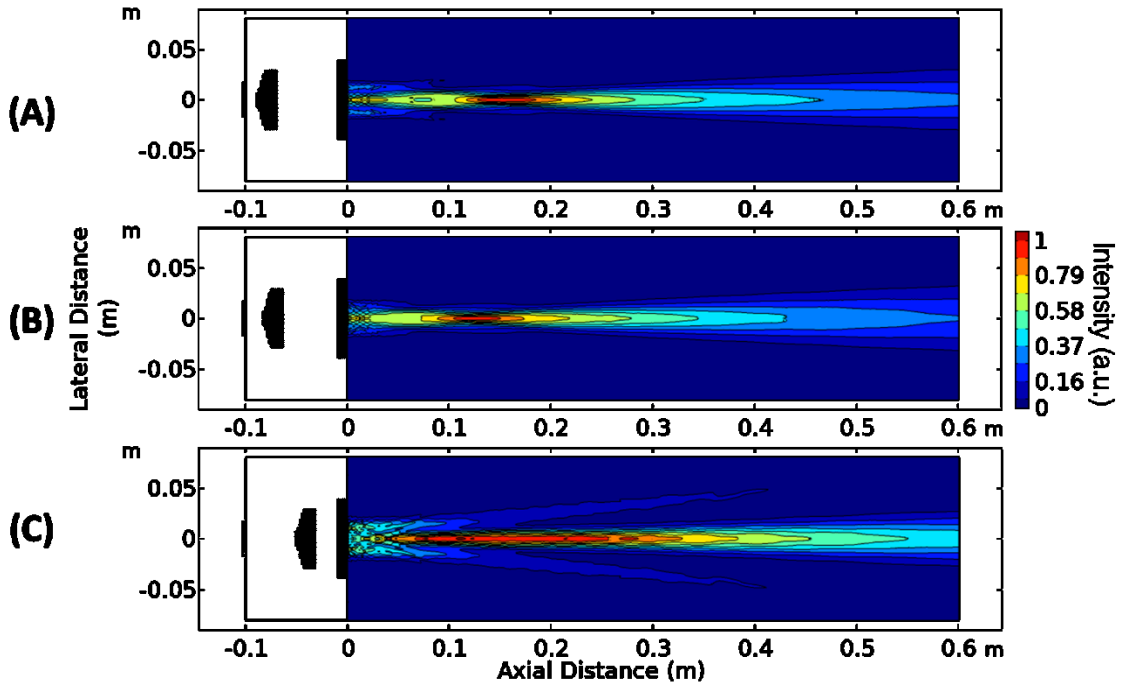

Figure 1. Numerical simulation of the doublet lens system performed tunable focusing (A) and (B), and collimation behavior (C).

2.2. Numerical simulation

Numerical simulations were performed using finite element analysis COMSOL multi-physics software. The transducer surface was located at 100 mm from the second lens element's outer edge in the model. The trapezoid lens element can be linearly translated between the transducer surface and the second flat lens. The doublet lens's behavior can be grouped into three distinct

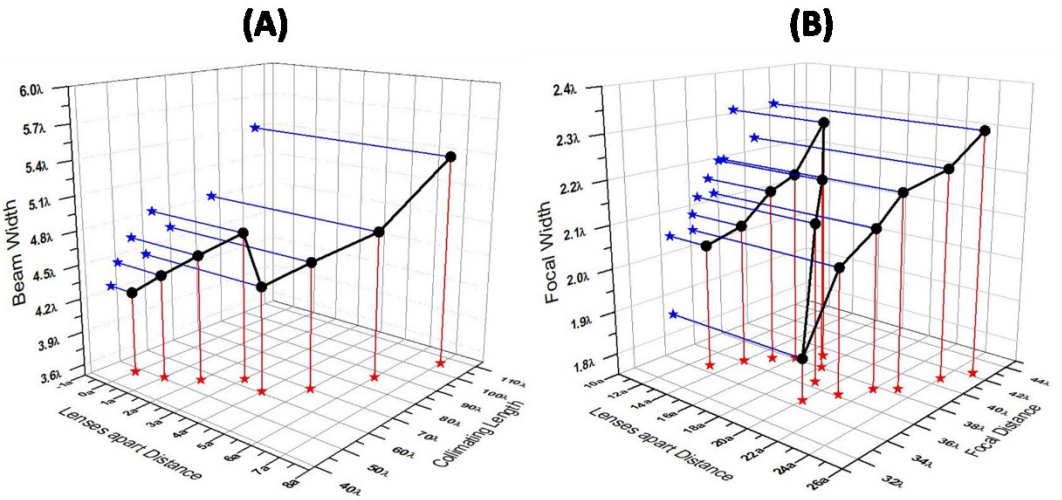

Figure 2. Numerical simulation based tunable collimation (A) and focusing (B) behavior of doublet lens system at various distances between the trapezoid and the planar element of the doublet [termed as "lens-apart distance"] (A) The collimation behavior from lens-apart distance 0a to 7a in terms of beam width and collimating length. (B) The tunable focusing behavior from lenes-apart distance 13a to 25a in terms of focal width and focal distance.

categories based on the relative position between the first lens and the near field focal point. When the two elements of the doublet lenses are 20a or more apart, a narrow focusing spot can be formed at a distance of 0.18m to 0.12m from the front edge of the second element of the lens. Figure 1 (A) and (B) demonstrated the focusing expected from a doublet lens when the trapezoidal and the rectangular elements are 25a and 20a distance apart. Under these conditions, the trapezoid shape lens is located before the near-field focal point of the transducer. When the distance between the two lens elements is reduced from 12a to 8a, additional focal points appear along the propagation axis. As the plano-convex lens element moved closer to the second lens (within 7a), the beam is focused on multiple spots along the propagation axis and appears as a collimation beam. Under these conditions, the plano-convex lens element crosses the center of the transducer's near-field focal point. Beyond the near-field limit, the focal point and collimation of the wave along the propagation axis do not follow a linear behavior. Figure 2 summarizes the collimation and focusing behaviors illustrated in (A) and (B) based on the simulated results. Figure 1 (C) illustrates that the most extended collimation of the beam occurs when the distance between the two-elements of the doublet lens is at 7a. The collimation distance is 175λ long and occurs from about 25 mm to 400 mm in figure 1C. The subsequent section's experimental results reveal that the transducer's finite size limits the beam dispersion to a collimation length of 77λ, which translates to 45 mm to 240 mm along the propagation axis.

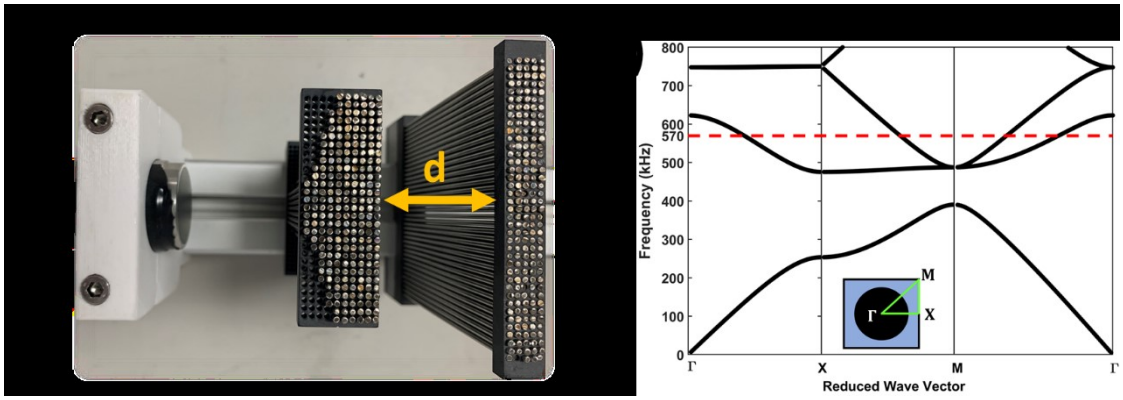

Figure 3. (A) Photograph of the mechanical tunable doublet lens system. The distance between the trapezoidal piece of the lens and the planar rectangular piece of the lens has been defined as "d" (B) Calculated band structure of the periodical water square lattice with circular stainless-steel scatter. The operating frequency was designed at 570 kHz located in the second transmission band.

3. Result and Discussion

3.1. Experimental Characterization of Doublet Meta-lenes

We fabricated the meta-lens as Figure 3 (A) illustrated. The holder plates were 3D printed by UV curing resin at 50μm resolution, which has very close acoustic properties to water to eliminate random scattering and reflection. The operating frequency, including the focusing and collimation of the dual meta-lens, is 570 kHz. This operation frequency is located within the structure's 2nd transmission band, as shown in Figure 3 (B). Similar characteristics can occur in the range of the second band ranging from 560 to 590 kHz. Figure 4 showed the experimentally measured spatial sound fields, which agreed with the simulation results showed

in Figure 1. The experimentally mapped area was 200 mm x 32 mm, which was the center of the mapped area and was located 150 mm away from the second lens's front edge. The tunable focal point was obtained at 110mm for a d = 25a (separation between the 1st and the 2nd element of the doublet lens) (Figure 4 (A)). The focal distance was reduced to 90mm for a distance d = 20a (Figure 4 (B)). A 190mm long collimation beam was also experimentally measured from 50mm to 240mm along the propagation axis, as shown in Figure 4 (C) for d = 7a.

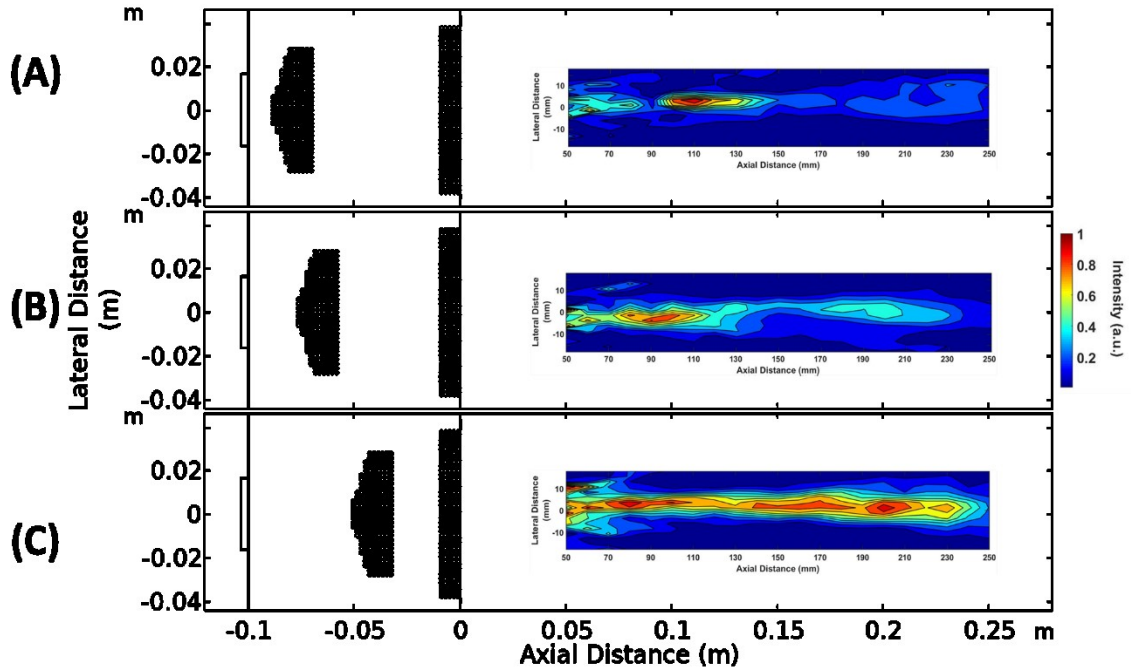

Figure 4. Experimentally mapped sound intensity field of the doublet lens system performed tunable focusing (A) and (B), and collimation behavior (C).

Figure 5 showed the focal width (A) and collimating beam width (B) analysis based on our simulation and experimental results. In Figure 5(A), the lateral sound intensity profile of the far focus was compared with the simulated results and shown in Figure 1 (A) and Figure 4 (A). The experimentally measured full width at half maximum (FWHM) was well agreed with a numerical simulation result of about 6mm, which is 2.2 λ. In the collimation configuration depicted in Figure 5 (B), the collimated beam from the doublet-lens system was experimentally measured as about FWHM 15mm (5.7 λ). It agreed with the simulation, 90 mm away from the front edge of the second element of the lens. Over 46 λ distance from 90mm to 210mm, the simulation showed almost no spreading in the FWHM beam intensity profile, and the experimental result showed about 1 mm spreading in collimation beamwidth.

For the frequency regions of focusing, the measured FWHM reduces from 20 mm (7 λ) in water ambient without the lens to 6 mm (2.2 λ) with the lens. The term Rayleigh length can provide a good estimation of the expected beam divergence, which is defined as $z_r = \frac{\pi w_0^2}{\lambda}$, where w_o is the radial beamwidth. Based on the measured results, we find that the Rayleigh length for the transducer zone to be z_{TA} =37.4λ, and with lens $z_{ML} = 3.14\lambda$. The emission source was a planar ultrasonic transducer with an active area piezoelectric material of 25.4mm.

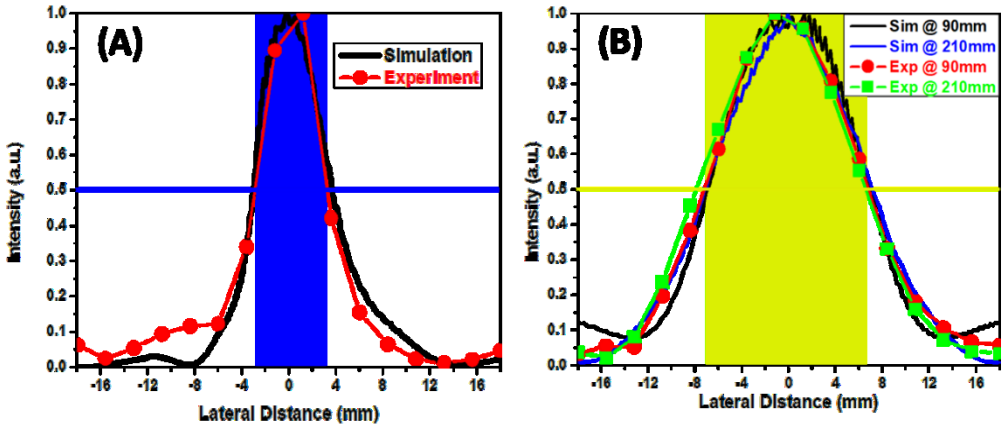

Figure 5. (A) Focal width of the far focusing in Figure 1 (A) and Figure 4 (A). (B) Collimation beam width and spreading analysis based on the simulation and experimental results from Figure 1 (B) and Figure 4 (B).

The range of the Fresnel zone is often referred to as the near field for the ultrasonic source. Near-field length L is defined as $L = \frac{D^2}{4\lambda}$, where D is the diameter of the transducer. At 570 kHz of the collimation frequency, the doublet lens yields a near-field length of L=60 mm. With the doublet lens, the collimation experimentally occurs within a range of 145-330 mm. The beam diverges by about 14% within the scanned cross-section starting from the surface of the transducer. In the axial direction, the strongest signal intensity with the narrowest beamwidth was detected around 295mm, which corresponds to 113.5λ past the Fresnel zone.

The doublet lens's tunable focusing and multi-focusing behavior resulting in a long collimating beam are demonstrated by experimental mapping of the acoustic wave's phase map within the area between the two lenses. To verify the different wave path occurred when the first locating inside or outside of the source transducer's near field zone, we scanned the sound wave phase

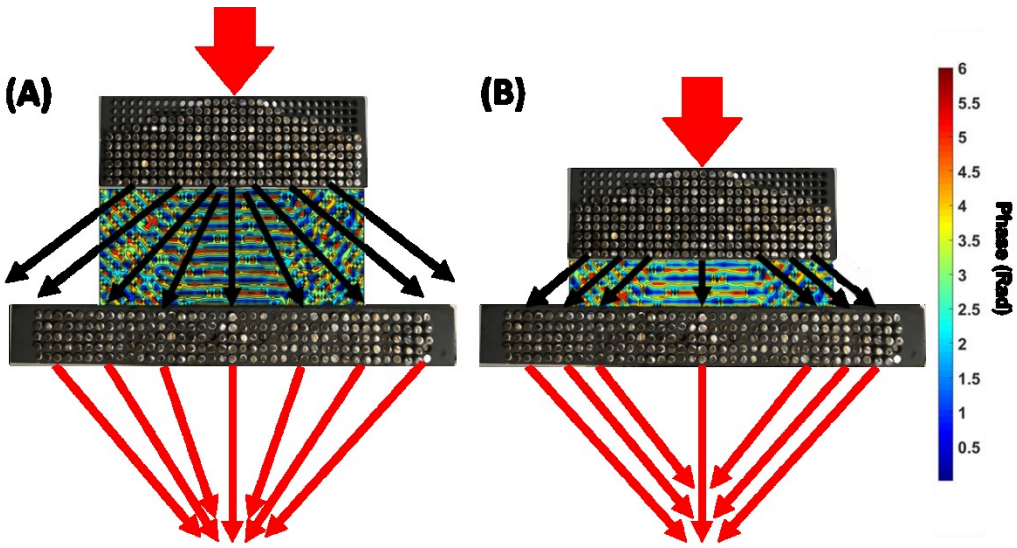

Figure 6. Experimentally measured 570 kHz phase map of focusing lens separation distance (A) and collimating lens separation distance (B). The transducer position was fixed in both cases which was 100 mm away the wider flat lens.

maps with different distance between the first lens and source transducer. The phase map in (A) is from a 60mm x 40mm area. And (B) showed a 60mm x14mm area of the wave phase between the two lenses in a collimation configuration. In the phase maps, the color scale indicates the measured wave phase from 0 to 2π (in radians). Figure 6 (A) indicated that the narrow focusing behavior occurred when the distance between the trapezoidal and the flat phononic structures was d=25a apart. Figure 6 (B) indicated that the long collimating behavior occurred when the distance between the trapezoidal and the flat phononic structures was d=7a apart. The incoherent wave transmitted through the first lens has a propagation direction normal to the blue to red transient in the phase maps. In Figure 6 (A), the second lens had incident waves with various incidence angles varying from 90° to about 50° over half the second component of the lens's surface area. As the figure depicts, the refracted wave from the second lens also undergoes refraction with the refracted angles varying from 90° (at the center of the lens) to about 50° (at the second edges lens). These results demonstrate limiting the dimension of the focusing spot along the axial direction due to the correlation of the angle of incidence due to the first lens and the refraction angle due to the second lens. In the collimation geometry (Figure 6 (B)), the phase map shows that the propagating wave's phase variation after the refraction from the trapezoidal lens is fairly uniformly incident on the second lens. The refraction due to the second lens occurs at various points along the axial direction and translates into a collimating beam. The mapped arrows in Figure 5 indicated the estimated wave path and explained the focusing and collimating behaviors.

3.2. Enhanced High-resolution Detection Experiments with Doublet meta-lens

The performance of the doublet-lens was analyzed for both organic and inorganic samples. Two 3D printed rods array samples were scanned laterally to compare the doublet-lens' relative performance to the transducer in the water environment. The results were stated in Figure 7 (monostatic detection) and Figure 8 (Bistatic detection). The inorganic sample for testing object size resolution (Sample 1) was a single 3D printed sample of 7 cylindrical rods of decreasing size 6mm to 1mm spaced at the equal interval, 16mm spacing. The inorganic sample for testing object spacing resolution (Sample 2) consisted of six pairs of rods of equal size (5 mm), spaced at decreasing distances from 19mm to 1.5mm. Complete explanations of the scanned samples and experimental setup are given in Methods and Materials (section 4). The two sets of samples provide the resolution of the size and the object spacing. Sample 1 is suited for comparing acuity, and sample 2 demonstrates the lateral resolution to determine the minimum separable width. Our ability to detect a single object is characterized by acuity and its lateral resolution to identify the correct number of closeby objects in this work.

3.2.1 Far-field Monostatic Detection

The practical application of ultrasonic detection uses a monostatic device in which the emitter acts as a detector simultaneously. Therefore, we tested the acuity and lateral resolution of the doublet-lens with a monostatic setup. In Figure 7, the inorganic sample 1 and sample 2 was scanned in the monostatic setup by collecting the reflected signal intensity. Figures 7 (C) and (D) showed the results scanned by the plane wave transducer with the doublet lens system. The samples were placed 40 mm away apart from the second lens, which was 140mm away from the transducer's surface. For comparison, the samples were scanned by the only transducer

without the doublet lens system. However, the reflected signal was barely detected correctly when the transducer was 140mm away from the samples. The beam from the source transducer spreads dramatically from around 18 λ. Without our lens, when the distance between transducer and sample was set to 53.8λ, the reflection back from side water tank walls and the actual echo from the sample were superposed in the record temporal data, which introduced uncertainty in the experiments. To overcome this limitation, the authors decided to use a closer transducer-to-sample distance to narrow down the time recorded window, and distance 15.4λ was selected to provide a relevant comparison.

Figures 7 (C) and (D) showed the two printed ABS samples' scanned results by the plane wave transducer without the doublet-lens system in 40mm distance between the transducer surface and the samples. Comparing Figures 7 (C), (E), and (D), (F), the doublet-lens system significantly enhanced the resolution and clarity of the detection quality. By the only transducer, the scan barely distinguished the separation and location of the small width objects from 2.6mm to 1mm, one$-\lambda$ to sub-wavelength. With the doublet-lens, the small rods' locations were well probed with the slightly wider size of the detected rods due to the large beamwidth of the collimation beam (15mm). Without the doublet lens enhancement, in sample 2, the transducer scan showed incorrect object locations, and the objects were not distinguished as separated rods for spacing less than 3mm. With the collimation beam offered by the doublet-lens system, the smallest designed separation distance between the rods in sample 2, 1.5mm, was properly detected. The locations of rods in sample 2 were also all correct.

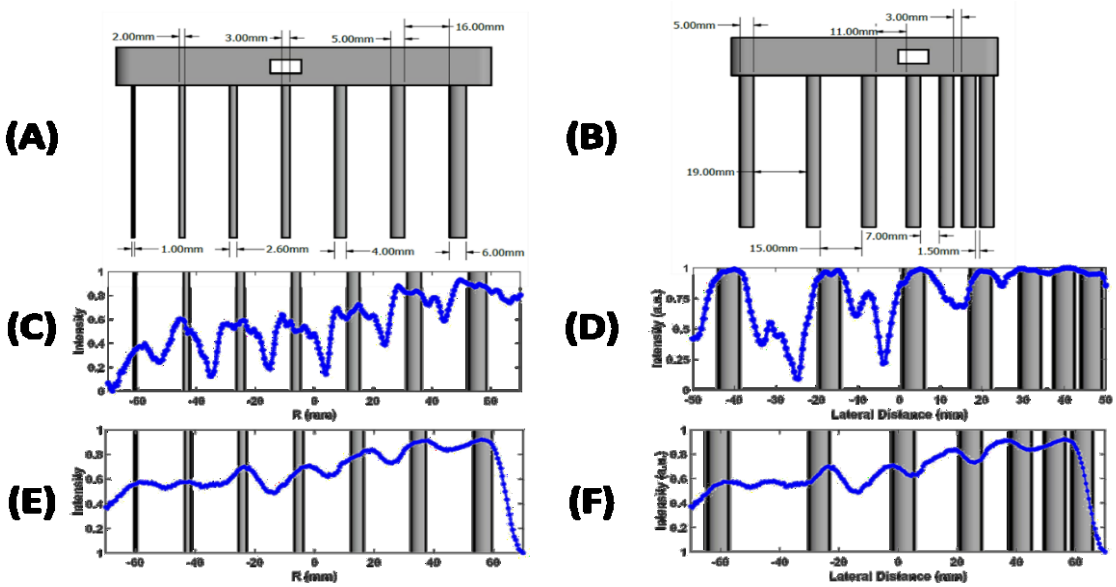

Figure 7. Monostatic detection of ABS 3D printed rods to examined monostatic detection resolution in terms of object size and edge-to-edge spacing. (A) Designed sample for size resolution test. (B) Designed sample for spacing resolution test. (C) Detection results of size resolution with the doublet lens system by its collimation. (D) Detection results of spacing resolution with the doublet lens system by its collimation. (E) Detection results of size resolution without the doublet lens, only transducer itself. (F) Detection results of spacing resolution without the doublet lens, only transducer itself. In (C) and (D), the sample was placed 15.4λ apart from the front lens, and transducer was 53.8λ away from the sample. In (E) and (F), the sample was placed 15.4λ apart transducer.

3.2.2. Super Far-field Bistatic Detection

In Fig. 8, the results were from the bistatic setup. In this experiment, the transducer was only the emission source. The detector was a needle style hydrophone, which was placed behind the samples (rods). The difference between the signal to noise ratio was due to the smaller piezo element on the hydrophone rather than the transducer. Figure 8 illustrated the super far-field bistatic detection of the plastic rods sample 1 and sample 2 in the over 70λ+ distance, which has never been reported in the existing literature of meta-lens applications. In (C) and (D), the sample was placed 80.4λ (210mm) apart from the front lens, and the transducer was 119.2λ (310mm) away from the scanned sample. In (E) and (F), the sample was placed 119.2λ apart transducer. In either case, the transducer only detection could not resolve two distinct objects, even if the rods were spaced much larger than one wavelength. The doublet-lens could resolve two different items clearly for five pairs out of 6 (From 7.3 λ to 1.15 λ), and they are all in the correct position. The smallest spacing is 1.5 mm; there is a small drop around -41mm (on lateral axis) in the figure, but it was not very clear. The measurement of acuity and lateral resolution for the emitting transducer alone was contaminated by boundary-reflected and sample-scattering noise due to the significant spread beam. The signal to noise ratio was low to

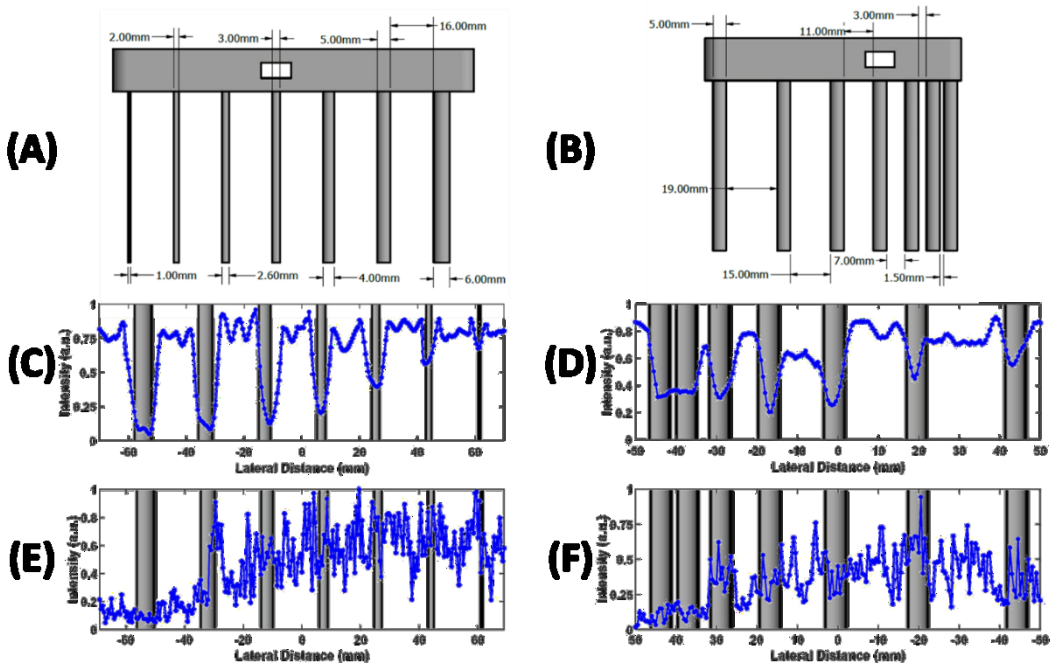

Figure 8. Bistatic detection of ABS 3D printed rods to examined bistatic detection resolution in terms of object size and edge-to-edge spacing. (A) Designed sample for size resolution test. (B) Designed sample for spacing resolution test. (C) Detection results of size resolution with the doublet lens system by its collimation. (D) Detection results of spacing resolution with the doublet lens system by its collimation. (E) Detection results of size resolution without the doublet lens, only transducer itself. (F) Detection results of spacing resolution without the doublet lens, only transducer itself. In (C) and (D), the sample was placed 80.4λ apart from the front lens, and transducer was 119.2λ away from the sample. In (E) and (F), the sample was placed 119.2λ apart transducer.

distinguish any of the rods individually in both samples. With the metamaterial doublet lens, each rod can be clearly distinguished by a sharp drop in a signal at the edges of each rod. The size and position are comparable with each rod. The detection of this bistatic detection of sample 1 was much more apparent than the previous monostatic measurement due to the receiver's small size (0.5mm width). The higher energy density collimated beam from the twin-lens system in super far-field detected the objects accurately. This object cannot be detected due to the relatively low energy density of the waves from a conventional transducer in the doublet lens's absence.

Gelatin tissue phantoms are good alternative materials for studying ultrasound imaging performance and investigating the doublet lens's compatibility in actual human tissues. The doublet-lens' detection quality in gelatin tissue phantoms was evaluated using bistatic arrangements in the super far-field, 80.4 λ away from the second lens's front edge. The tissue phantoms have been developed according to the procedures. Two hard objects and mass objects of tissue of various sizes and compositions were synthesized into tissue phantoms to compare the doublet-lens' characterization capability and the transducer alone. Carrot tissue embedded in gelatin tissue phantoms served as bistatic samples, where the lens was stationary while a lateral translation stage swept the samples.

Sample 3 (tested for object size resolution) consists of five carrot rods, in the widths of 2.3mm (0.88 λ), 6.1mm (2.34 λ), 6.3mm (2.42 λ), 8.5mm (3.26 λ), and 12.1mm (4.65 λ) for testing size resolution showed in Figure 9 (A). Sample 4 (tested for object spacing resolution)

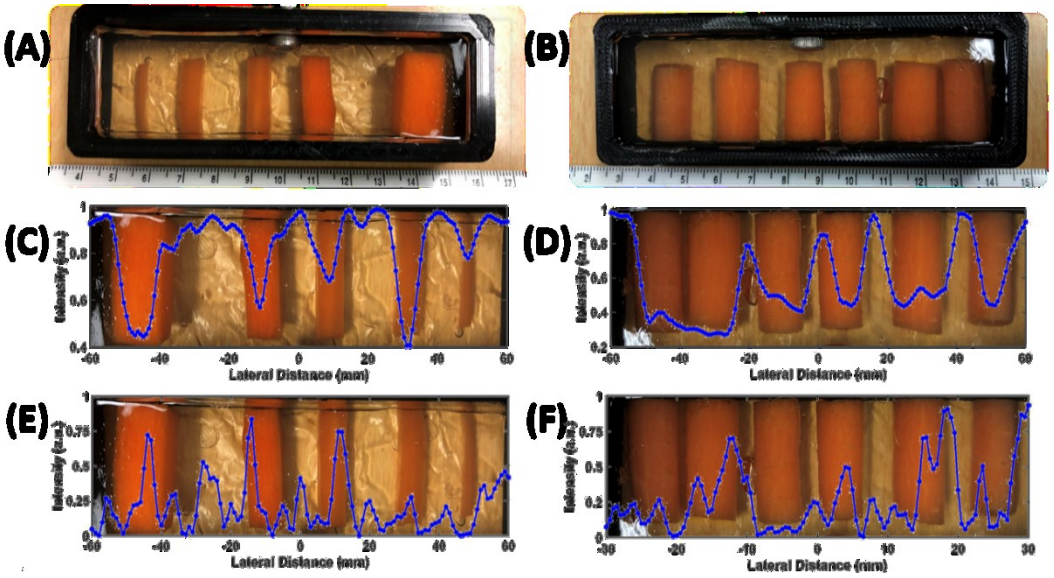

Figure 9. Bistatic detection of organic mass samples to examined bistatic detection resolution in terms of object size and edge-to-edge spacing. (A) Designed sample for size resolution test. (B) Designed sample for spacing resolution test. (C) Detection results of size resolution with the doublet lens system by its collimation. (D) Detection results of spacing resolution with the doublet lens system by its collimation. (E) Detection results of size resolution without the doublet lens, only transducer itself. (F) Detection results of spacing resolution without the doublet lens, only transducer itself. In (C) and (D), the sample was placed 80.4λ apart from the front lens, and transducer was 119.2λ away from the sample. In (E) and (F), the sample was placed 119.2λ apart transducer.

has five pair of carrot biomass in the distance between are 1.6mm (0.62 λ), 3.1mm (1.19 λ), 3.8mm (1.46 λ), 5.3mm (2.03 λ), and 7.1mm (2.73 λ) to exam spacing resolution presented in Figure 9 (A). Samples 3 were mainly used to analyze the resolving power or acuity of the doublet lens, while sample 4 was used to evaluate lateral resolution as it pertains to measurable minimum separable space. Figures 9 (C), (D), (E), and (F) showed the comparison between the transducer along and with the doublet lens. Sample 3 was scanned, and the results showed in (C) with the doublet lens and (E) without the doublet lens. Sample 4 was detected and presented in (D) with the doublet lens and (F) without the doublet lens. In all four experiments, the transducer was 310mm away from the samples. With the doublet lens, detection obtained the smallest carrot in gelatin was 2.3mm. The sample 3 scan with lens showed all correct carrots' correct location and well-estimated carrots width in Figure 9 (C). In Figure 9 (D), the 1.6mm spacing was detected but not clearly. Besides the smallest spacing, other carrots in detected results were all in the correct location. The error of carrot width might be caused by the difference in the orientation of the square cross-section carrots slabs. The transducer alone could not show the presence of objects since the hydrophone could not collect any transmitted signal through the gelatin carrots samples after such a long distance due to large attenuation from the samples. In (E) and (F), the transducer only scans the detected signal considered as the background noise in equipment, which had averaged energy level of about -95 dBm before linearization and normalization. On the other hand, the doublet-lens detected the size and positions of each of the masses accurately.

3.3. Discussion

From the existing literature, many parameters are used to estimate the performance of a lens, including full width at half maximum (FWHM), size resolution, and spacing resolution [21, 22, 23, 24]. To summarize the metamaterial doublet-lens system's behavior, including focusing and collimating, and comparing our doublet lens system's performance with other metamaterial lenses in the existing literature, we compared the parameters of metamaterial acoustic lenses in terms of focal width and focal length. The summarized information was normalized with its operational wavelength and is shown in Figure 10. The red circle represented Phononic crystal-based lens [25] [26] [27] [28] [15]. The blue square stands for Fresnel lens, gradient index planar lens, and liquid-filled membrane lens [29] [30] [31] [32] [33]; the Green triangle is a hollow 2D structure and hollow 3D structure with a negative index of refraction [34] [35]. The pink diamond refers to a hyperbolic metamaterial lens [36]. The black star refers to the doublet-lens system. Some exciting trends between the phononic crystal-based lens were concluded. On the left, a sharper curve between focal length and focal distance illustrated by conventional phononic crystal based metamaterial lenses with square lattice or modified square lattice without special designs. Most of them have square lattice with circular scatters, which has an immense slope on the focusing width or the spot size with increased focal length. The relatively less sharp slope dash line shows advance designed phononic crystal-based meta-lens based on gradient filling fraction used to enhance the focal length with a relatively less broadening of the spot size. The doublet-lens system demonstrated in this work has the most extended focal length among existing lenses with a relatively small focal width in the existing meta-lens in the literature.

A recent study used a pair of lenses based on the asymmetric unit cells meta-surface lens focused on a narrow point in the near field. [38]. However, the asymmetric unit cell design introduced the limitation of this lens in a monostatic configuration. In the meta-surface work, due to their asymmetric unit cell design, the possibility of a monostatic detection was limited by its non-reciprocity or asymmetric transmission. In our doublet-lens, the lattices are fully symmetric. The doublet-lens in this study demonstrates sub-wavelength lateral resolution 15λ+ past the Fresnel zone in a monostatic setup. The long working distance focusing and collimation introduced the potential to achieve practical deep tissue detection in future practical applications. In the far distance (70 λ+), the bistatic detection resolution is still outstanding, about one wavelength. These advantages of the doublet-lens have not been demonstrated in any existing acoustic meta-lens.

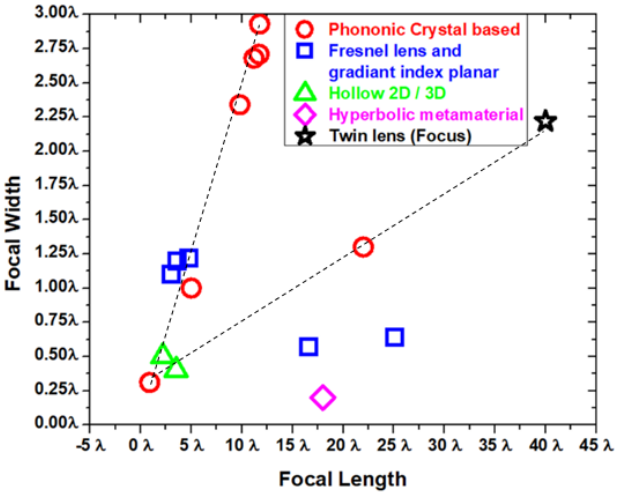

Figure 10. Focusing behavior comparison between the Doublet lens system in this study and other existing acoustic meta-material from the literature in terms of focal length and focal width.

4. Materials and experimental setup

4.1. Mapping and detection

As Figure 11 (A) shows, the bistatic experiment for the far-field characterization of the lens's lateral resolution. Due to the limitation of the equipment, the reflected signal is barely detected without an amplifier over almost 200 λ round-trip distance. The bistatic experiment was performed in the inorganic material system and tissue phantoms with a single element 1-inch Panametrics V301 unfocused immersion transducer. The Muëller-Platte 0.5 mm Needle Probe hydrophone acted as the detector. During the experiment, the sample was moved using a linear translation stage. Simultaneously, the hydrophones, lenses, and transducer were well aligned in the same axis and subsequently kept static for lateral scans. The samples were then translated and raster-scanned between the hydrophone and the lens. The experiments were performed with and without the lens. Bistatic measurement and detection consisted of continuous 565-575 kHz wave sweep in frequency analyzer mode on Tektronix MDO3024b in a big water tank (1.5m by 0.9m by 0.6m).

Figure 11 (B) illustrated the monostatic spectroscopic pulse-echo reflection measurements and were performed with an emitter-connected imaging DPR300 pulse receptor. Data were collected with a fixed lens, and the analyzed samples were swept in front of the lens using a lateral translating stage. The experiment was conducted within a room temperature small water tank (0.5m by 0.5m by 0.5m). The pulsing data consisting of 512 average signals in Tektronix MDO3024b. The frequency information was from the Fourier Transform.

In Fig. 7, the figures presented monostatic detection. The transducer worked as both an emission source and a detector. The collected signals were the reflection from the sample (rods). In Fig. 8, the results were from the bistatic setup. In this experiment, the transducer was only the emission source. The detector was a needle style hydrophone which was placed behind the samples (rods). The difference between the signal to noise ratio contributed from the smaller piezo element on the hydrophone rather than the transducer.

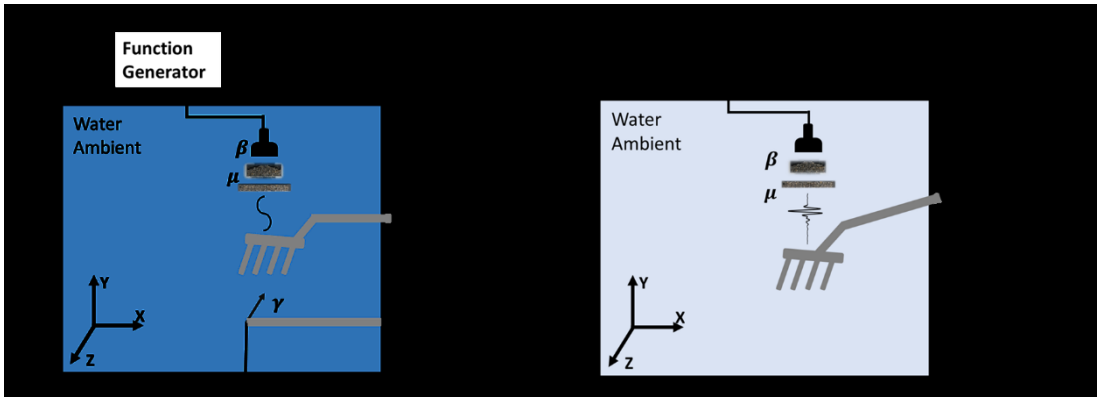

Figure 11. (A) Bistatic measurements setup for bistatic detection. Sound intensity field mapped in the same setup without sample between the lens and needle hydrophone detector. (B) Monostatic measurements setup for monostatic detection.

4.2. Inorganic ABS samples

Acrylonitrile butadiene styrene (ABS) rods were printed using a 3D printer to measure the doublet lens range and spatial resolution. The rods were printed with a 0.2 mm diameter printing nozzle with a Polyprinter 229 filament with ABS under a 100% filled environment. Sample 1 consisted of seven rods with diameters of 6mm, 5mm, 4mm, 3mm, 2.6mm, 2mm, and 1mm. Sample 2 consisted of seven rods with variable spacing between the adjacent cylindrical rods. The variable spacing is 19mm, 15mm, 11mm, 7mm, 3mm, and 1.5mm. Both sample 1 and sample 2 were in water ambient. The emitter and lens were set for each measurement, and the samples were swept over a range of 60 mm from the emitter in front of the lens. The reflection was measured against the location of the sample and recorded.

4.3. Organic samples

Gelatin tissue phantoms were made using a standard synthesis procedure. [39]. The gelatin was made with 1000 ml of water, in which 32 small bags (220 g) of KNOX. Eight boxes were added to the water and heated to 50 ° C. The remaining boxes were then added slowly and blended perfectly to attain a viscous and homogeneous solution mixture. The gelatin solution was then put into a 3D printed container and cooled under room temperature to avoid bubbles. After it cooled down to room temperature, the gelatin solution was placed in a refrigerator for 24 hours. The organic size resolution sample consisted of five carrot mass cuts to widths of 2.3mm ($0.88\ \lambda$), 6.1mm ($2.34\ \lambda$), 6.3mm ($2.42\ \lambda$), 8.5mm ($3.26\ \lambda$), and 12.1mm ($4.65\ \lambda$). The size was evaluated by Image J software to measure the size resolution. Five pairs of carrots of about 10 mm in width were placed within the same tissue phantom to evaluate the doublet lens's spatial resolution capabilities in the bistatic arrangement. Analysis using Image J showed

that the distances between the paired biomasses were estimated to be 1.6mm (0.26 λ), 3.1mm (1.19 λ), 3.8mm (1.46 λ), 5.3mm (2.03 λ), and 7.1mm (2.73 λ).

5. Conclusion

This study proposed the first metamaterial lens that demonstrates both tunable focusing and collimating behavior in a super far-field limit. The experimental results are agreed with the numerical simulation results. The two-component phononic crystal based acoustic meta-material lens is a simplistic design that can be fabricated using a periodic arrangement of metallic rods without any complex geometrical lens shaping. The doublet lens has a long focal length that extended up to 42.3 λ away from the lens's surface and could be tuned to 36.5 λ by linear mechanical translation of one of the lens's linear components. By further varying the distance between the lenses' component, a long collimation distance of 71 λ was realized, which offered far-field detection in the experiments. In the far-field limit, the novel lens structure can spatially resolve inorganic objects up to 0.26 λ with a separation of 0.58 λ resolution in the monostatic setup. These objects were at a distance of 15 λ from the lens. In an organic material, the lens can detect an object that is 80 λ away with a spatial resolution of 0.62 λ resolution of size and 1.15 λ separation in a bistatic configuration. The novel lens opens up the potential of non-destructive analysis of detection and imaging objects in the far-field limit with super-resolution capabilities. The tunable doublet lens provided a solution to overcome the metamaterial behaving limitation, either focusing or collimating. This functionality makes the acoustic metamaterial lens approached closer to the practical detection applications, which normally finished by a tunable phased array transducer. Moreover, the 80 wavelengths away organic samples detection capability introduced the potential of the acoustic metamaterial lens.

6. Acknowledgement

This work is supported by an Emerging Frontiers in Research and Innovation (EFRI) grant from the National Science Foundation (NSF Grant No. 1741677). The support from the infrastructure and support of the Center for Agile & Adaptive and Additive Manufacturing (CAAAM) funded through the State of Texas Appropriation #190405-105-805008-220 is also gratefully acknowledged.

References

[1] Y. Wu and Z.-Q. Zhang, "Dispersion relations and their symmetry properties of electromagnetic and elastic metamaterials in two dimensions," *Phys. Rev. B,* vol. 79, no. 195111, 2009.

[2] C. Shen, Y. Xie, N. Sui, W. Wang, S. Cummer and Y. Jing, "Broadband Acoustic Hyperbolic Metamaterial," *Phys. Rev. Lett.,* vol. 115, no. 254301, 2015.

[3] Y. Zubov, B. Djafari-Rouhani, Y. Jin, M. Sofield, E. Walker, A. Neogi and A. Krokhin, "Long-range nonspreading propagation of sound beam through periodic layered structure," *Communications Physics,* vol. 3, no. 1, pp. 1-8, 2020.

[4] S. Tol, F. L. Degertekin and A. Erturk, "Gradient-index phononic crystal lens-based enhancement of elastic wave energy harvesting," *Appl. Phys. Lett.,* vol. 109, 2016.

[5] H. He, C. Qiu, L. Ye, X. Cai, X. Fan, M. Ke, F. Zhang and Z. Liu, "Topological negative refraction of surface acoustic waves in a Weyl phononic crystal," *Nature,* vol. 560, 2018.

[6] M.-H. Lu, L. Feng and Y.-F. Chen, "Phononic crystals and acoustic metamaterials," *Materials today,* vol. 12, no. 12, pp. 34-42, 2009.

[7] Y.-F. Chen, P. Fischer and F. W. Wise, "Negative refraction at optical frequencies in nonmagnetic two-component molecular media," *Physical review letters,* vol. 95, no. 6, p. 067402, 2005.

[8] S. H. Lee and O. B. Wright, "Origin of negative density and modulus in acoustic metamaterials," *Physical Review B,* vol. 93, no. 6, p. 024302, 2016.

[9] J. E. R. Bucay, J. O. Vasseur, P. A. Deymier, A. C. Hladky-Hennion, Y. Pennec, K. Muralidharan, B. Djafari-Rouhani and B. Dubus, "Positive, negative, zero refraction, and beam splitting in a solid/air phononic crystal: Theoretical and experimental study," *Physical Review B,* vol. 79, no. 21, p. 214305, 2009.

[10] Y. Jin, E. Walker, A. Krokhin, H. Heo, T.-Y. Choi and A. Neogi, "Enhanced Instantaneous Elastography in Tissues and Hard Materials Using Bulk Modulus and Density Determined without Externally Applied Material Deformation," *IEEE transactions on ultrasonics, ferroelectrics, and frequency control,* vol. 67, no. 3, pp. 624 - 634, 2019.

[11] Y. Jin, E. Walker, H. Heo, A. Krokhin, T. Y. Choi and A. Neogi, "Nondestructive ultrasonic evaluation of fused deposition modeling based additively manufactured 3D-printed structures," *Smart Materials and Structures,* vol. 29, no. 4, p. 045020, 2020.

[12] Y. Jin, T. Yang, H. Heo, A. Krokhin, S. Q. Shi, N. Dahotre, T.-Y. Choi and A. Neogi, "Novel 2D Dynamic Elasticity Maps for Inspection of Anisotropic Properties in Fused Deposition Modeling Objects," *Polymers,* vol. 12, no. 9, p. 1966, 2020.

[13] E. L. Walker, D. Reyes-Contreras, Y. Jin and A. Neogi, "Tunable Hybrid Phononic Crystal Lens Using Thermo-Acoustic Polymers," *ACS omega,* vol. 4, no. 15, pp. 16585-16590, 2019.

[14] E. L. Walker, Z. Wang and A. Neogi, "Radio-frequency actuated polymer-based phononic meta-materials for control of ultrasonic waves," *NPG Asia Materials,* vol. 9, no. 2, p. e350, 2017.

[15] C. Qiu, X. Zhang and Z. Liu, "Far-field imaging of acoustic waves by a two-dimensional sonic crystal," *Physical Review B,* vol. 71, no. 5, p. 054302, 2005.

[16] J. Zhu, J. Christensen, J. Jung, L. Martin-Moreno, X. Yin, L. Fok, X. Zhang and F. J. Garcia-Vidal,

"A holey-structured metamaterial for acoustic deep-subwavelength imaging," *Nature Physics,* vol. 7, pp. 52-55, 2011.

[17] A. Sukhovich, B. Merheb, K. Muralidharan, J. Vasseur, Y. Pennec, P. Deymier and J. Page, "Experimental and Theoretical Evicence for Subwavelength Imaging in Phononic Crystals," *Phys. Rev. Lett.,* vol. 102, no. 154301, 2009.

[18] J. Li, F. Wu, H. Zhong, Y. Yao and X. Zhang, "Acoustic beam splitting in two-dimensional phononic crystals using self-collimation effect," *Journal of Applied Physics,* vol. 118, no. 14, p. 144903, 2015.

[19] J. Bucay, E. Roussel, J. O. Vasseur, P. A. Deymier, A. C. Hladky-Hennion, Y. Pennec, K. Muralidharan, B. B. Djafari-Rouhani and B. Dubus, "Positive, negative, zero refraction, and beam splitting in a solid/air phononic crystal: Theoretical and experimental study," *Physical Review B,* vol. 79, no. 21, p. 214305, 2009.

[20] E. Walker, D. Reyes, M. M. Rojas, A. Krokhin and A. Neogi, "Funneled focusing of planar acoustic waves utilizing the metamaterial properties of an acoustic lens," *Proc. SPIE 8994, Photonic and Phononic Properties of Engineered Nanostructures IV,* vol. 89940H, 2014.

[21] K. Diamantis, A. Greenaway, T. Anderson, J. A. Jensen and V. Sboros, "Experimental performance assessment of the sub-band minimum variance beamformer for ultrasound imaging," *Ultrasonics,* vol. 79, pp. 87-95, 2017.

[22] J. Liu, Q. He and J. Luo, "A compressed Sensing Strategy for Synthetic Transmit Aperture Ultrasound Imaging," *IEEE Transactions on Medical Imaging,* vol. 36, no. 4, 2017.

[23] S. Chen and K. Parker, "Enhanced axial and lateral resolution using stabilized pulses," *J. Med Imag.,* vol. 42, no. 2, 2017.

[24] S. Chen and K. Parker, "Enhanced resolution pulse-echo imaging with stabilized pulses," *J. Med. Imag.,* vol. 3, no. 2, 2016.

[25] L. Bai, G. Y. Song, W. X. Jiang, Q. Cheng and T. J. Cui, "Acoustic tunable metamaterials based on anisotropic unit cells," *Applied Physics Letters,* vol. 115, no. 23, p. 231902, 2019.

[26] S. Peng, Z. He, H. Jia, A. Zhang, C. Qiu, M. Ke and Z. Liu, "Acoustic far-field focusing effect for two-dimensional graded negative refractive-index sonic crystals," *Applied Physics Letters,* vol. 96, no. 26, p. 263502, 2010.

[27] T. P. Martin, M. Nicholas, G. J. Orris, L.-W. Cai, D. Torrent and J. Sánchez-Dehesa, "Sonic gradient index lens for aqueous applications," *Applied Physics Letters,* vol. 97, no. 11, p. 113503, 2010.

[28] Y. Kanno, K. Tsuruta, K. Fujimori, H. Fukano and S. Nogi, "Phononic-Crystal Acoustic Lens by Design for Energy-Transmission Devices," *Electronics and Communications in Japan,* vol. 97, no. 1, pp. 22-27, 2014.

[29] J. Chen, J. Xiao, D. Lisevych, A. Shakouri and Z. Fan, "Deep-subwavelength control of acoustic waves in an ultra-compact metasurface lens," *Nature communications,* vol. 9, no. 1, pp. 1-9, 2018.

[30] J. Zhao, H. Ye, K. Huang, Z. N. Chen, B. Li and C.-W. Qiu, "Manipulation of acoustic focusing with an active and configurable planar metasurface transducer," *Scientific reports,* vol. 4, p. 6257, 2014.

[31] J. Hyun, Y. T. Kim, I. Doh, B. Ahn, K. Baik and S.-H. Kim, "Realization of an ultrathin acoustic lens for subwavelength focusing in the megasonic range," *Scientific reports,* vol. 8, no. 1, pp. 1-

12, 2018.

[32] D. Tarrazó-Serrano, C. Rubio, O. V. Minin, P. Candelas and I. V. Minin, "Manipulation of focal patterns in acoustic Soret type zone plate lens by using reference radius/phase effect," *Ultrasonics,* vol. 91, pp. 237-241, 2019.

[33] L. Zigoneanu, B.-I. Popa and S. A. Cummer, "Design and measurements of a broadband two-dimensional acoustic lens," *Physical Review B,* vol. 84, no. 2, p. 024305, 2011.

[34] J. Lopes, M. Andrade, J. Leao-Neto, J. Adamowski, I. Minin and G. Silva, "Focusing acoustic beams with a ball-shaped lens beyond the diffraction limit," *Physical Review Applied,* vol. 8, no. 2, p. 024013, 2017.

[35] J.-p. Xia, X.-t. Zhang, H.-x. Sun, S.-q. Yuan, J. Qian and Y. Ge, "Broadband tunable acoustic asymmetric focusing lens from dual-layer metasurfaces," *Physical Review Applied,* vol. 10, no. 1, p. 014016, 2018.

[36] J. Christensen and F. J. G. de Abajo, "Anisotropic metamaterials for full control of acoustic waves," *Physical review letters,* vol. 108, no. 12, p. 124301, 2012.

[37] J. H. Lopes, M. A. B. Andrade, J. P. Leao-Neto, J. C. Adamowski, I. V. Minin and G. T. Silva, "Focusing acoustic beams with a ball-shaped lens beyond the diffraction limit," *Physical Review Applied,* vol. 8, no. 2, p. 024013, 2017.

[38] J.-p. Xia, X.-t. Zhang, H.-x. Sun, S.-q. Yuan, J. Qian and Y. Ge, "Broadband tunable acoustic asymmetric focusing lens from dual-layer metasurfaces," *Physical Review Applied ,* vol. 10, no. 1, p. 014016, 2018.

[39] R. Bude and R. Adler, "An Easily Made, Low-Cost, Tissue-Like Ultrasound Phantom Material," *J. Clin. Ultrasound,* vol. 23, pp. 271-273, 1995.